

# Resistively detected electron spin resonance and $g$ factor in few-layer exfoliated MoS<sub>2</sub> devices

Chithra H. Sharma<sup>1,2\*</sup>, Appanna Parvangada<sup>2</sup>, Lars Tiemann<sup>2</sup>, Kai Rossnagel<sup>1,3</sup>, Jens Martin<sup>4</sup>, Robert H. Blick<sup>2,5</sup>

<sup>1</sup>*Institut für Experimentelle und Angewandte Physik, Christian-Albrechts-Universität zu Kiel, 24098 Kiel, Germany*

<sup>2</sup>*Center for Hybrid Nanostructures (CHyN), Universität Hamburg, Luruper Chaussee 149, 22761 Hamburg, Germany*

<sup>3</sup>*Ruprecht Haensel Laboratory, Deutsches Elektronen-Synchrotron DESY, 22607 Hamburg, Germany*  
<sup>4</sup>*Leibniz Institut für Kristallzüchtung, 12489 Berlin, Germany*

<sup>5</sup>*Material Science and Engineering, University of Wisconsin-Madison, University Ave. 1550, Madison, 53706, Wisconsin, USA*

\*Chithra.Sharma@physik.uni-hamburg.de

## Abstract

MoS<sub>2</sub> has recently emerged as a promising material for enabling quantum devices and spintronic applications. In this context, the demonstration of resistively detected electron spin resonance (RD-ESR) and the determination and improved physical understanding of the  $g$  factor are of great importance. However, its application and RD-ESR studies have been limited so far by Schottky or high-resistance contacts to MoS<sub>2</sub>. Here, we exploit naturally  $n$ -doped few-layer MoS<sub>2</sub> devices with ohmic tin (Sn) contacts that allow the electrical study of spin phenomena. Resonant excitation of electron spins and resistive detection is a possible path to exploit the spin effects in MoS<sub>2</sub> devices. Using RD-ESR, we determine the  $g$  factor of few-layer MoS<sub>2</sub> to be  $\sim 1.92$  and observe that the  $g$  factor value is independent of the charge carrier density within the limits of our measurements.

Electron spin resonance (ESR) is a powerful technique to investigate the behavior of electron spins and extract information such as  $g$  factor, spin-relaxation times, and spin-orbit interaction strength. In materials where resistively detected ESR (RD-ESR) can be used, the manipulation of the electron spins in a device environment can be studied. [1,2] Hence, RD-ESR is crucial for the development of spintronic devices, including spin valves and spin field-effect transistors (FETs). [3] Recently, RD-ESR has emerged as a tool to drive spin rotations, making it attractive for the control of spin qubits. [4]

Promising candidates in this regard are van der Waals (vdW) materials. Specifically, the semiconducting transition-metal dichalcogenides (TMDCs) such as MoS<sub>2</sub> are of prime interest due to their gate tunability, stability, and abundance. MoS<sub>2</sub>-based transistors as well as quantum dots realized by lateral electrostatic electron confinement have already been demonstrated. [5–9] Such devices could be used as a platform for nanoelectronics, optoelectronics, and spintronics. [10,11] Among other effects, spin-valley interactions in monolayer and twisted bilayer MoS<sub>2</sub> and proximity-induced spin-orbit coupling in graphene-MoS<sub>2</sub> heterostructures have been investigated. [2,12,13] Further, the potential of MoS<sub>2</sub> as a material for qubits in quantum computing has been explored. [14,15] Recent progress has also been made in wafer-scale device applications, positioning 2D-TMDCs on the industrial roadmap and making them a promising material platform for future quantum devices and technologies. [16,17]

RD-ESR is a useful tool for the advancement of spintronic devices based on 2D-vdW materials. RD-ESR has been used to determine the  $g$  factor in monolayer graphene and to measure the effects of intrinsic spin-orbit coupling and pseudospin in graphene devices. [1,18,19] In graphene/MoS<sub>2</sub> heterostructures, the modulation of the  $g$  factor of graphene in proximity to MoS<sub>2</sub> has been reported. [2] For monolayer MoS<sub>2</sub>, theory predicts an electron  $g$  factor ranging from 1.98 to 2.2 for the conduction band. [15] There are reports of ESR measurements on bulk MoS<sub>2</sub> samples utilizing conventional absorption spectroscopy. [20,21] Using conventional ESR spectroscopy on CVD-grown multilayer MoS<sub>2</sub> film devices with ionic gel gating, temperature-dependent  $g$  factors for various vacancies and defects in the range of 2.045 – 2.055 have been determined. [22] Alternatively, time-resolved Kerr rotation spectroscopy on CVD grown  $n$ -type MoS<sub>2</sub> revealed  $g$  factor in the range of 1.902 to 1.975. [23] Additionally, electronic transport in 1D-channels of split-gated MoS<sub>2</sub> devices was investigated and a  $g$  factor of 2.16 was extracted. [24] However, a strongly confined geometry can significantly affect the  $g$  factor, so the value cannot be assumed to be the intrinsic property of the material. [25]

To the best of our knowledge, RD-ESR has not yet been applied to measure the electron  $g$  factor in MoS<sub>2</sub>. RD-ESR measurements allow *in operando* measurements of “real” device geometries, but require high sensitivity to detect the subtle resistance changes. Especially for low-temperature experiments, large contact resistances and Schottky barriers have prevented direct  $g$  factor measurements in MoS<sub>2</sub> by ESR. Recently, several metals, including Indium (In) and Tin (Sn), have been shown to make ohmic contact with MoS<sub>2</sub>. [26–29] Specifically, Sn contacts deposited at low temperatures have shown ohmic contact resistances of only ~1-3 k $\Omega$   $\mu$ m. [28,29] In this work, we use thermally evaporated Sn deposited on liquid N<sub>2</sub>-cooled samples. Our few-layer MoS<sub>2</sub> devices show excellent device performance, as demonstrated and discussed below. We perform magneto-transport measurements and RD-ESR spectroscopy [1] to extract the electronic  $g$  factor in the conduction band of few-layer MoS<sub>2</sub>.

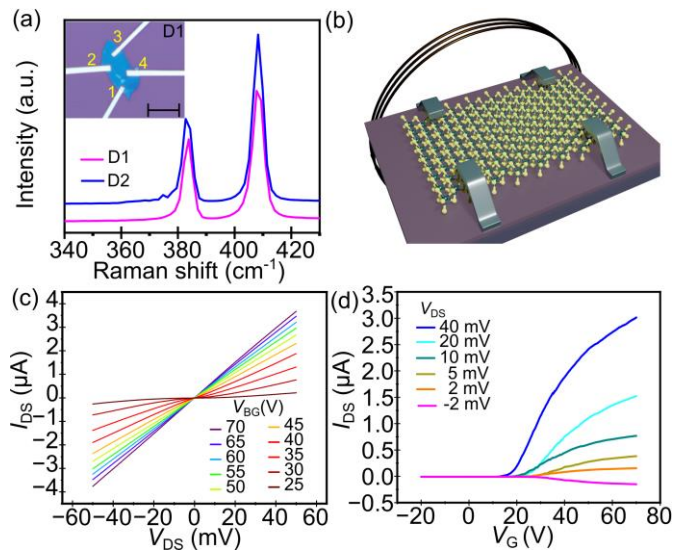


Fig. 1: (a) Raman spectra of the MoS<sub>2</sub> flakes showing the E<sub>12g</sub> and A<sub>1g</sub> peaks. Inset: optical image of the device D1 with Sn contacts and the contacts labeled from 1 to 4. Scale bar is 20  $\mu$ m. (b) Schematic of the experimental setup showing the device with the loop antenna. (c) Two-probe  $I$ - $V$  curves at ~1.6 K for different back-gate voltages ( $V_{BG}$ ) for D1. (d) Transconductance of the device D1 for different bias voltages ( $V_{DS}$ ) at ~1.6 K.

We investigated two devices, D1 and D2. The devices are fabricated by manually exfoliating few-layer MoS<sub>2</sub> flakes (8-12 layers by optical contrast [30]) and transferring them, using a PDMS-assisted dry transfer technique, to a *p*-doped Si wafer with 300 nm SiO<sub>2</sub> with prefabricated Ti/Au bonding pads. We used natural MoS<sub>2</sub> bulk material from SPI supplies. The ohmic contacts to MoS<sub>2</sub> were realized by e-beam lithography followed by Sn evaporation on a cooled sample [28] and lift-off. Figure 1(a) shows the Raman spectra of the flakes in the device D1 (magenta) and D2 (blue), where the positions of the E<sub>12g</sub><sup>1</sup> and A<sub>1g</sub> peaks can be read as 383.49 cm<sup>-1</sup> and 408.27 cm<sup>-1</sup>, respectively. The Raman spectra were recorded after the Sn deposition, indicating that the quality of the material was not compromised during the fabrication process. The optical image of device D1 is shown in the inset with the Sn contacts labeled from 1-4. After wire bonding, the devices were mounted on a vacuum probe (~10<sup>-5</sup> mbar) with minimal exposure to the atmosphere (<30 min) to avoid oxidation of the metal-semiconductor interface. Electrical transport measurements were performed at a temperature of ~1.6 K in a variable temperature insert in a cryostat equipped with a solenoid magnet and a loop antenna. A schematic of the device with a loop antenna for microwave irradiation is depicted in Fig. 1(b).

We first discuss the results for the D1 device. Figure 1(c) shows the *I*-*V* characteristics of the device for different gate voltages. The two-probe transconductance (contacts 2 and 4) at 1.6 K for different bias voltages is shown in Fig. 1(b). A linear behavior in the *I*-*V* can be observed for gate voltages of 45 V and above, where a saturation behavior of the transconductance can also be seen. We performed four-probe magnetotransport measurements at 1.6 K in the longitudinal (*I*<sub>14</sub>, *V*<sub>23</sub>) and transverse/Hall (*I*<sub>24</sub>, *V*<sub>13</sub>) configurations. The Hall measurements for different gate voltages for D1 are shown in Fig. 2(a). Weak localization behavior, as shown in the inset, was observed in *R*<sub>xx</sub>. Due to the asymmetry of the contacts, small longitudinal components lead to an offset and a superimposed weak localization. A narrow weak localization peak indicates good device quality and is typically seen only in encapsulated devices. [31–33]

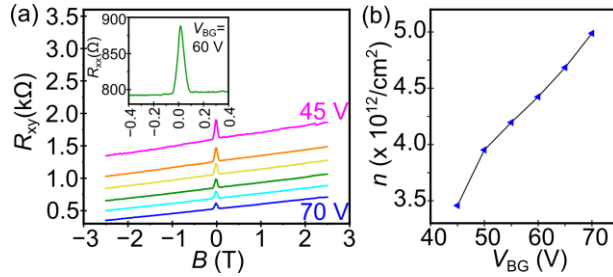


Fig. 2: (a) Magnetotransport measurement in Hall configuration for different gate voltages. The inset shows the weak-localization behavior in longitudinal mode at  $V_{BG} = 60.0 V$ . (b) Extracted Hall mobility (blue) and carrier densities (red) as a function of the gate voltage.

The Hall mobilities (left) and the carrier densities (right) extracted from the magnetotransport measurements for different gate voltages for D1 are shown in Fig. 2(b). The carrier densities were extracted from the slope of the Hall data and the mobility using the formula  $\mu = \frac{\sigma}{ne}$ , where  $n$  is the calculated carrier density,  $e$  is the electronic charge, and  $\sigma$  is the conductivity. We used  $\sigma = \frac{l}{w R_{xx}(B=0)}$ , where  $l = 33 \mu m$  is the distance between contacts 1 and 3 and  $w = 15 \mu m$  is the distance between the contacts 2 and 4. We extract carrier densities in the range of  $\sim 3.5\text{-}5 \times 10^{12} cm^{-2}$  for gate voltages of 45-70 V, where linear *I*-*V* is observed. The values are comparable to previously observed results in Sn-contacted MoS<sub>2</sub> devices. [28] We calculate a maximum mobility of  $\sim 2900 cm^2/Vs$  at  $V_{BG} = 70.0 V$  at 1.6 K, which is much higher than values reported in the literature for unencapsulated devices [31,34]

and comparable to many encapsulated devices. [32,35,36] We note that our measurement geometry deviates from the standard Hall bar and van der Pauw geometry. Therefore, the estimated mobility

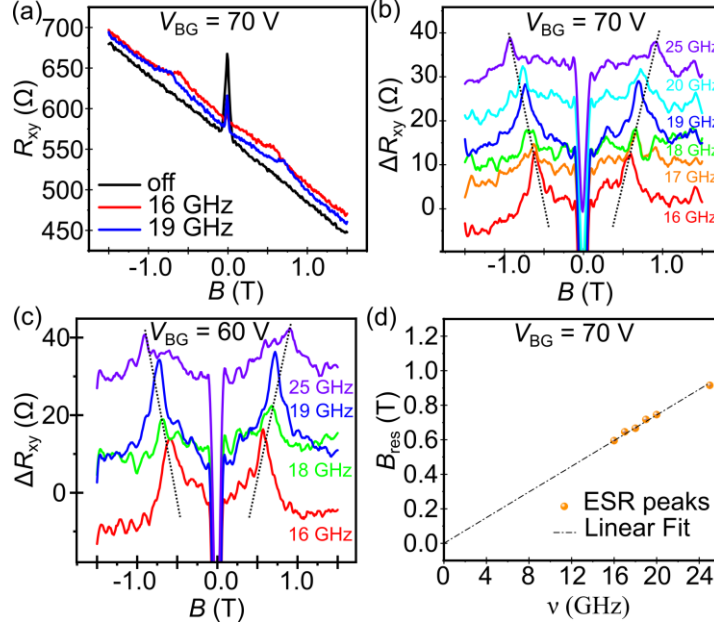


Fig. 3: (a) Hall data for microwave excitation off (black), 16.0 GHz (magenta), and 19.0 GHz (red) for D1 at  $V_g = 70.0$  V. Background subtracted data for different microwave excitations for D1 at (b)  $V_{BG} = 70.0$  V, (c)  $V_{BG} = 60.0$  V. (d) Extracted ESR peak positions for different excitation frequencies from (b).

should be taken as an upper limit, while the true mobility may be lower by a factor of 4. We did not increase the gate voltage beyond 70 V to avoid gate leakage and dielectric breakdown in this device.

For RD-ESR spectroscopy, we applied a microwave signal in the range of 15-26 GHz to a loop antenna as shown in the schematics in Fig. 1(b). A small change in the device resistance is observed due to resonant absorption of the spins in the magnetic field when  $h\nu = g\mu_B B_{res}$ , where  $\nu$  is the applied frequency,  $B_{res}$  is the external magnetic field at resonance,  $h$  and  $\mu_B$  are Planck's constant and Bohr magneton, respectively. Magnetotransport data in the Hall configuration with microwave excitations of 16 GHz (red) and 19 GHz (blue) are shown in Fig. 3(a) for device D1 at a gate voltage of 70.0 V. The curve in black shows the background where the microwave excitation is off [same as the blue curve in Fig. 2(a)]; *i.e.*,  $R_{xy}(off)$ . Clear ESR signals are observed in our samples. We choose the Hall configuration for the RD-ESR measurements because the linear background facilitates the observation and to maintain consistency. A change in the total device resistance is also observed during microwave excitation due to the heating effect. For clarity, background subtraction [*i.e.*,  $R_{xy}(\nu) - R_{xy}(off)$ ] was performed on the RD-ESR data, where Figs. 3(b) and 3(c) show results for different microwave excitations on device D1 for  $V_{BG} = 70.0$  V and  $V_{BG} = 60.0$  V, respectively. The curves are smoothed (Savitzky-Golay) and Lorentzian fits to the resonance peaks were used to extract the  $B_{res}$  for different frequencies. The extracted  $B_{res}$  from Fig. 3(b), plotted against the microwave excitation frequencies, are shown in Fig. 3(d). We extract a  $g$  factor of  $1.92 \pm 0.03$  for D1 at a gate voltage of 70.0 V. Similarly, we estimate a  $g$  factor of  $1.91 \pm 0.01$  for  $V_{BG} = 60.0$  V.

We also performed the measurements on a second device, D2. Interestingly, D2 showed a linear  $I$ - $V$  response even at  $V_{BG} = 0$  V, as shown in Fig. 4(a). Although there were no deliberate differences in

the processing of the different devices, we assume that the local differences in the bulk material or some differences in the contact formation could be the probable reasons for this behavior. The inset shows the optical image of the device with contacts labeled from 1 to 7. The  $I$ - $V$  curves for different pairs of contacts at 1.6 K are shown here (contacts 6 and 7 were not functional). Unfortunately, the device showed an onset of gate leakage above  $V_{BG} \approx 2V$ , and hence the gate was kept at  $V_{BG} = 0.0 V$  for further measurements to avoid any dielectric breakdown. We performed magnetotransport and RD-ESR measurements in the transverse/Hall ( $I_{13}$ ,  $V_{24}$ ) configuration at  $V_{BG} = 0.0 V$  for D2. A carrier

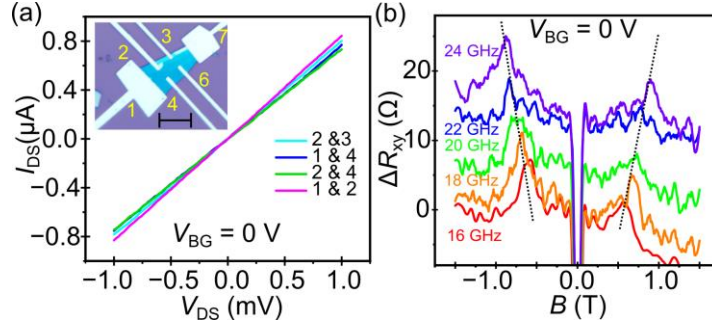


Fig. 4: (a) Two-probe  $I$ - $V$  curves at  $\sim 1.6 K$  for different contact pairs at  $V_{BG} = 0 V$  for D2. Optical image of D2 in the inset to (d); scale bar is  $10 \mu m$ . (b) Background subtracted data for different microwave excitations for D2 at  $V_{BG} = 0.0 V$ .

density of  $2.9 \times 10^{12} \text{ cm}^{-2}$  was measured (data not shown). Figure 4(b) shows the background subtracted ESR data and we estimate a  $g$  factor of  $1.92 \pm 0.02$  at  $V_{BG} = 0.0 V$ .

In summary, we have measured the effective  $g$  factor in few-layer  $\text{MoS}_2$  to be  $\sim 1.92$  through RD-ESR spectroscopy. The ohmic contact provided by Sn and the excellent device quality allowed us to make this measurement. Our measurements on two devices cover a range of carrier densities. However, we observed that the value of the  $g$  factor does not seem to have a significant dependence on the range of carrier densities studied, as summarized in Tab. 1. The variation of the densities is consistent with the gate capacitance of the dielectric, *i.e.*,  $n = \frac{C_{ox}}{e} V_{BG}$ , where  $C_{ox}$  is the gate capacitance ( $C_{ox} = \frac{\epsilon_r \epsilon_0}{d}$ ) and  $e$  is the electronic charge,  $\epsilon_r = 3.9$  is the dielectric constant for  $\text{SiO}_2$  and  $d = 300 \text{ nm}$  is the thickness of the dielectric. Hence, we can assume that the two devices had the same doping. We find a  $g$  factor that is significantly lower than theoretical predictions as well as most other experimental results using other gating techniques. Similar measurements on graphene have also shown different  $g$  factors than those measured by RD-ESR. [1,37] The possible variation in the measurement environment and the material could be a reason for this and that needs to be further investigated.

Considering the significant spin-orbit coupling (SOC) [36] in the conduction band (much lower than in the valence band), the  $g$  factor is surprisingly close to that of graphene ( $\sim 1.95$ ) and the free electron  $g$  factor ( $\sim 2.0023$ ). While SOC is a determining factor, other factors such as spin-valley coupling, hyperfine coupling, exchange interactions, defects and impurities would also influence the spin properties. We expect that our measurements will pave the way for further studies to shed light on

Device	$V_{BG}$ (V)	Carrier density ( $\text{cm}^{-2}$ )	$g$ factor
D1	70.0	$(4.988 \pm 0.001) \times 10^{12}$	$1.92 \pm 0.03$
D1	60.0	$(4.423 \pm 0.001) \times 10^{12}$	$1.91 \pm 0.01$
D2	0.0	$(2.902 \pm 0.009) \times 10^{12}$	$1.92 \pm 0.02$

Tab. 1: Summary of measured  $g$  factors.

these as well as  $g$  factor anisotropy, substrate dependence, the effect of doping, strain, etc., which need to be explored in more detail in MoS<sub>2</sub>. RD-ESR measurements with higher frequency ranges would also be interesting to probe the SOC gap in the system. [18] Our experiments have demonstrated that specially tailored MoS<sub>2</sub> devices can resistively detect and control spin effects, enabling advanced studies for spintronics and qubit applications.

## Acknowledgements

We thank Christian Schäfer (IKZ Berlin) for tin (Sn) deposition. We thank the Excellence Cluster CUI-AIM for support (EXC 2056).

## Author Declarations

The authors have no conflicts to disclose.

## Data availability

The data that support the findings of this study are available from the corresponding author upon reasonable request.

## References

- [1] T. J. Lyon, J. Sichau, A. Dorn, A. Centeno, A. Pesquera, A. Zurutuza, and R. H. Blick, *Probing Electron Spin Resonance in Monolayer Graphene*, Phys. Rev. Lett. **119**, 066802 (2017).
- [2] C. H. Sharma, P. Zhao, L. Tiemann, M. Prada, A. D. Pandey, A. Stierle, and R. H. Blick, *Electron Spin Resonance in a Proximity-Coupled MoS<sub>2</sub>/Graphene van Der Waals Heterostructure*, AIP Adv. **12**, 035111 (2022).
- [3] Y. K. Luo, J. Xu, T. Zhu, G. Wu, E. J. McCormick, W. Zhan, M. R. Neupane, and R. K. Kawakami, *Opto-Valleytronic Spin Injection in Monolayer MoS<sub>2</sub>/Few-Layer Graphene Hybrid Spin Valves*, Nano Lett. **17**, 3877 (2017).
- [4] K. C. Nowack, F. H. L. Koppens, Y. V. Nazarov, and L. M. K. Vandersypen, *Coherent Control of a Single Electron Spin with Electric Fields.*, Science **318**, 1430 (2007).
- [5] C. H. Sharma and M. Thalakulam, *Split-Gated Point-Contact for Electrostatic Confinement of Transport in MoS<sub>2</sub>/h-BN Hybrid Structures*, Sci. Rep. **7**, 735 (2017).
- [6] R. Pisoni, Y. Lee, H. Overweg, M. Eich, P. Simonet, K. Watanabe, T. Taniguchi, R. Gorbachev, T. Ihn, and K. Ensslin, *Gate-Defined One-Dimensional Channel and Broken Symmetry States in MoS<sub>2</sub> van Der Waals Heterostructures*, Nano Lett. **17**, 5008 (2017).
- [7] R. Pisoni, Z. Lei, P. Back, M. Eich, H. Overweg, Y. Lee, K. Watanabe, T. Taniguchi, T. Ihn, and K. Ensslin, *Gate-Tunable Quantum Dot in a High Quality Single Layer MoS<sub>2</sub> Van Der Waals Heterostructure*, Appl. Phys. Lett. **112**, 123101 (2018).
- [8] Z.-Z. Zhang et al., *Electrotunable Artificial Molecules Based on van Der Waals Heterostructures*, Sci. Adv. **3**, e1701699 (2017).
- [9] A. Sebastian, R. Pendurthi, T. H. Choudhury, J. M. Redwing, and S. Das, *Benchmarking Monolayer MoS<sub>2</sub> and WS<sub>2</sub> Field-Effect Transistors*, Nat. Commun. **12**, 693 (2021).
- [10] R. Ganatra and Q. Zhang, *Few-Layer MoS<sub>2</sub>: A Promising Layered Semiconductor*, ACS Nano **8**, 4074 (2014).
- [11] Q. H. Wang, K. Kalantar-Zadeh, A. Kis, J. N. Coleman, and M. S. Strano, *Electronics and Optoelectronics of Two-Dimensional Transition Metal Dichalcogenides.*, Nat. Nanotechnol. **7**, 699 (2012).
- [12] R. Pisoni et al., *Interactions and Magnetotransport through Spin-Valley Coupled Landau Levels in Monolayer MoS<sub>2</sub>*, arXiv:1806, (2018).
- [13] C. H. Sharma, M. Prada, J.-H. Schmidt, I. González Díaz-Palacio, T. Stauber, T. Taniguchi, K. Watanabe, L. Tiemann, and R. H. Blick, *Transport Spectroscopy Study of Minibands in MoS<sub>2</sub> Moiré Superlattices*, Phys. Rev. B **109**, 195106 (2024).
- [14] J. Pawłowski, *Spin-Valley System in a Gated MoS<sub>2</sub>-Monolayer Quantum Dot*, New J. Phys. **21**, 123029 (2019).

- [15] A. Kormányos, V. Zólyomi, N. D. Drummond, and G. Burkard, *Spin-Orbit Coupling, Quantum Dots, and Qubits in Monolayer Transition Metal Dichalcogenides*, Phys. Rev. X **4**, 011034 (2014).
- [16] F. Giustino et al., *The 2021 Quantum Materials Roadmap*, JPhys Mater. **3**, 042006 (2020).
- [17] Y. Y. Chung et al., *First Demonstration of GAA Monolayer-MoS<sub>2</sub> Nanosheet NFET with 410 μm ID 1V VD at 40nm Gate Length*, in *Technical Digest - International Electron Devices Meeting, IEDM*, Vols. 2022-Decem (2022), pp. 34.5.1-34.5.4.
- [18] J. Sichau, M. Prada, T. Anlauf, T. J. Lyon, B. Bosnjak, L. Tiemann, and R. H. Blick, *Resonance Microwave Measurements of an Intrinsic Spin-Orbit Coupling Gap in Graphene: A Possible Indication of a Topological State*, Phys. Rev. Lett. **112**, 046403 (2019).
- [19] R. G. Mani, J. Hankinson, C. Berger, and W. A. De Heer, *Observation of Resistively Detected Hole Spin Resonance and Zero-Field Pseudo-Spin Splitting in Epitaxial Graphene*, Nat. Commun. **3**, 996 (2012).
- [20] A. Stesmans, S. Iacovo, and V. V. Afanas'Ev, *ESR Study of P-Type Natural 2H-Polytype MoS<sub>2</sub> Crystals: The As Acceptor Activity*, Appl. Phys. Lett. **109**, 172104 (2016).
- [21] A. Stesmans, B. Schoenaers, and V. V. Afanas'ev, *Variations of Paramagnetic Defects and Dopants in Geo-MoS<sub>2</sub> from Diverse Localities Probed by ESR*, J. Chem. Phys. **152**, 234702 (2020).
- [22] N. Tsunetomo, S. Iguchi, M. Wierzbowska, A. Ueda, Y. Won, S. Heo, Y. Jeong, Y. Wakayama, and K. Marumoto, *Spin-States in MoS<sub>2</sub> Thin-Film Transistors Distinguished by Operando Electron Spin Resonance*, Commun. Mater. **2**, 27 (2021).
- [23] L. Yang, W. Chen, K. M. McCreary, B. T. Jonker, J. Lou, and S. A. Crooker, *Spin Coherence and Dephasing of Localized Electrons in Monolayer MoS<sub>2</sub>*, Nano Lett. **15**, 8250 (2015).
- [24] K. Marinov, A. Avsar, K. Watanabe, T. Taniguchi, and A. Kis, *Resolving the Spin Splitting in the Conduction Band of Monolayer MoS*, Nat. Commun. (2017).
- [25] K. J. Thomas, J. T. Nicholls, M. Y. Simmons, M. Pepper, D. R. Mace, and D. A. Ritchie, *Possible Spin Polarization in a One-Dimensional Electron Gas*, Phys. Rev. Lett. **77**, 135 (1996).
- [26] B. K. Kim, T. H. Kim, D. H. Choi, H. Kim, K. Watanabe, T. Taniguchi, H. Rho, J. J. Kim, Y. H. Kim, and M. H. Bae, *Origins of Genuine Ohmic van Der Waals Contact between Indium and MoS<sub>2</sub>*, Npj 2D Mater. Appl. **5**, 9 (2021).
- [27] A. Shanmugam, M. A. Thekke Purayil, S. A. Dhurjati, and M. Thalakulam, *Physical Vapor Deposition-Free Scalable High-Efficiency Electrical Contacts to MoS<sub>2</sub>*, Nanotechnology **35**, 115201 (2024).
- [28] Z. Cao, F. Lin, G. Gong, H. Chen, and J. Martin, *Low Schottky Barrier Contacts to 2H-MoS<sub>2</sub> by Sn Electrodes*, Appl. Phys. Lett. **116**, 133104 (2020).
- [29] A. S. Chou et al., *High On-State Current in Chemical Vapor Deposited Monolayer MoS<sub>2</sub>nFETs with Sn Ohmic Contacts*, IEEE Electron Device Lett. **42**, 272 (2021).
- [30] and M. T. A. Varghese, C. H. Sharma, *Topography Preserved Microwave Plasma Etching for Top-down Layer Engineering in MoS<sub>2</sub> and Other van Der Waals Materials [Supplementary Material]*, Nanoscale **9**, 3818 (2017).
- [31] A. T. Neal, H. Liu, J. J. Gu, and P. D. Ye, *Magneto-Transport in MoS<sub>2</sub>: Phase Coherence, Spin-Orbit Scattering, and the Hall Factor*, ACS Nano **7**, 7077 (2013).
- [32] N. Papadopoulos, K. Watanabe, T. Taniguchi, H. S. J. Van Der Zant, and G. A. Steele, *Weak Localization in Boron Nitride Encapsulated Bilayer MoS<sub>2</sub>*, Phys. Rev. B **99**, 115414 (2019).
- [33] T. Qu, M. Masseroni, T. Taniguchi, K. Watanabe, B. Özyilmaz, T. Ihn, and K. Ensslin, *Observation of Weak Localization in Dual-Gated Bilayer Mo S<sub>2</sub>*, Phys. Rev. Res. **6**, 013216 (2024).
- [34] B. Baugher, H. O. H. Churchill, Y. Yang, and P. Jarillo-Herrero, *Intrinsic Electronic Transport Properties of High Quality Monolayer and Bilayer MoS<sub>2</sub>*, Nano Lett. **13**, 4212 (2013).
- [35] M. Masseroni, T. Qu, T. Taniguchi, K. Watanabe, T. Ihn, and K. Ensslin, *Evidence of the Coulomb Gap in the Density of States of MoS<sub>2</sub>*, Phys. Rev. Res. **5**, 013113 (2023).
- [36] R. Pisoni et al., *Interactions and Magnetotransport through Spin-Valley Coupled Landau Levels in Monolayer MoS<sub>2</sub>*, Phys. Rev. Lett. **121**, 247701 (2018).
- [37] N. Fujita, D. Matsumoto, Y. Sakurai, K. Kawahara, H. Ago, T. Takenobu, and K. Marumoto, *Direct Observation of Electrically Induced Pauli Paramagnetism in Single-Layer Graphene Using ESR Spectroscopy*, Sci. Rep. **6**, 34966 (2016).